Semi-Supervised Anomaly Detection in Directed Energy Deposition Using Thermal Images

Ufuk Ismail Ozdek, Yigit Kaan Tonkaz, Shawqi Mohammed Farea and Mustafa Unel

Faculty of Engineering and Natural Sciences, Sabancı University, Istanbul, Turkey

Keywords: Additive Manufacturing, Directed Energy Deposition (DED), Anomaly Detection, Semi-Supervised Learning,

One-Class Support Vector Machine (OCSVM), Isolation Forest (iForest).

Abstract: Directed Energy Deposition (DED) is a crucial additive manufacturing process used in aerospace and health-

care applications, among others. However, ensuring defect-free production remains a challenge due to the difficulty in detecting defect-related anomalies in real-time. In this study, we address the problem of defect detection in DED processes through thermal images of melt pools. As an anomaly detection problem, we adopt a semi-supervised approach based on One-Class Support Vector Machine (OCSVM) and Isolation Forest (iForest). We analyze the performance of these models across different feature sets. Additionally, this semi-supervised approach is compared against an unsupervised approach utilizing the same learning algorithms. The results indicate the superiority of the semi-supervised approach for both algorithms. Yet, iForest outperforms OCSVM with an accuracy of 95% and an F1-score of 0.88, demonstrating its robustness in distinguishing defective from non-defective instances. This work provides valuable insights into the applicability of semi-supervised machine learning techniques for real-time defect detection in DED processes. By leveraging thermal imaging data and feature-based anomaly detection models, our findings contribute to the development

of efficient, non-destructive quality control mechanisms for additive manufacturing processes.

1 INTRODUCTION

Additive manufacturing (AM) has revolutionized the production of complex metal components in industries such as aerospace, healthcare, and defense (Dass and Moridi, 2019). Among various AM techniques, Directed Energy Deposition (DED) offers unique advantages in producing large-scale, high-strength parts due to its ability to deposit material layer-bylayer with controlled thermal input (Li et al., 2023). However, ensuring the structural integrity of DEDmanufactured components remains a significant challenge due to the formation of in-situ defects such as porosity, cracking, and lack of fusion. These defects, if undetected, compromise the mechanical properties of the final product and necessitate expensive postproduction inspections, increasing both costs and material waste (Tang et al., 2022). Traditional defect detection methods, such as X-ray Computed Tomography (XCT) and destructive testing, are timeconsuming and impractical for real-time monitoring. While process maps and optimized printing parameters can reduce defects, they do not eliminate them entirely due to variations in machine settings, material properties, and environmental factors. Therefore, real-time, non-destructive anomaly detection is crucial for improving the quality and reliability of DED-printed parts (Zamiela et al., 2023b; Herzog et al., 2024).

Machine learning-based approaches provide a promising alternative by enabling real-time, non-destructive defect detection, thereby reducing reliance on post-production inspections. While machine learning (ML) techniques have been extensively explored for defect detection in additive manufacturing, their application to DED remains comparatively underdeveloped (Hespeler et al., 2022; Qin et al., 2022), with most research focusing on Powder Bed Fusion (PBF) and Selective Laser Melting (SLM). ML-based anomaly detection in DED is still evolving, with promising potential for enhancing product quality.

Among ML approaches, supervised methods, such as support vector machines (SVM) and convolutional neural networks (CNN), achieve high accuracy in classifying defects in DED processes using thermal images. However, they require extensive labeled datasets, which are resource-intensive to obtain (Gaja and Liou, 2018; Khanzadeh et al., 2018). In

contrast, unsupervised techniques have gained significant attention for defect detection in DED processes due to their ability to analyze large amounts of unlabeled data and identify hidden patterns associated with defects. Techniques such as K-means clustering, self-organizing maps (SOM), density-based spatial clustering of applications with noise (DBSCAN), and principal component analysis (PCA) are commonly used to detect anomalies in process data (Taheri et al., 2019; García-Moreno, 2019; Farea et al., 2024). Additionally, unsupervised deep learning methods, such as Variational Autoencoders (VAE), have been explored for capturing complex, non-linear relationships in DED thermal imaging data. VAE has been used to encode high-dimensional thermal images into a latent space, reconstructing input images and identifying defects by analyzing reconstruction errors (Zhao et al., 2021). Gaussian mixture model (GMM) and K-means clustering techniques have been applied to these latent representations to further refine anomaly detection in melt pools, allowing models to separate defective and normal regions effectively.

Recent studies have also focused on selfsupervised learning techniques, such as Masked Autoencoders (MAE) and Vision Transformers (ViT), to enhance feature extraction from unlabeled melt pool data (Era et al., 2024). MAE has been pretrained on thermal images, where a portion of the image was masked and reconstructed, enabling the model to capture robust spatial dependencies without requiring labeled data. After pretraining, finetuned MAE was successfully integrated with supervised classifiers, such as CNN and Multi-Layer Perceptron (MLP) models, to detect melt pool anomalies. These advancements underscore the potential of self-supervised learning and deep generative models in enhancing real-time, unsupervised defect detection in DED, reducing reliance on large labeled datasets, and improving the scalability of in-situ quality control frameworks (Era et al., 2024).

However, the formulation of DED defect detection as a semi-supervised learning problem remains underexplored. This formulation offers a distinct advantage over supervised and unsupervised methods, particularly in handling data imbalance. As with most anomaly detection tasks, DED defect detection datasets are imbalanced, with defective instances representing only a small fraction of the data. In a semi-supervised framework, models are trained exclusively on normal data to learn the underlying distribution of normal behavior, where significant deviations from this distribution are classified as anomalies. This approach enhances robustness against data imbalance compared to supervised and unsupervised methods.

In this work, we formulate defect detection in DED processes as a semi-supervised learning problem, employing two effective semi-supervised algorithms: One-Class Support Vector Machine (OCSVM) and Isolation Forest (iForest). To effectively model the normal behavior of defect-free data, we implement preprocessing steps such as segmentation and domain knowledge-driven feature engineering.

The remainder of the paper is organized as follows: Section 2 details the proposed methodology, including preprocessing steps and semi-supervised models. Section 3 presents the experimental results and discussion, while Section 4 provides the concluding remarks.

2 METHODOLOGY

The methodological framework, shown in Figure 1, is structured around two anomaly detection models-OCSVM and iForest. These models were selected based on their capability to detect anomalies in environments where labeled defect data is scarce, a common constraint in DED quality control. OCSVM models the normal class boundary, while iForest isolates outliers through random splits. Compared to deep learning-based semi-supervised models (e.g., semi-supervised VAE), shallow models such as OCSVM and iForest offer several advantages—especially in structured data settings. These include greater computational efficiency, easier integration of domain knowledge via preprocessing and feature engineering, enhanced interpretability, and simpler hyperparameter tuning.

2.1 Threshold Segmentation

Threshold segmentation was applied to extract the melt pool region from the thermal images. A threshold of 1640 °C was used, corresponding to the liquidus temperature of the feedstock material (Ti-6Al-4V). This segmentation enables the localization of the melt pool boundary and facilitates the feature extraction relevant to thermal distribution and shape analysis (Alexopoulou, 2021).

2.2 Feature Extraction

Three comprehensive categories of features were extracted from the thermal melt pool images:

1) **Statistical Features:** A set of descriptive statistics was computed from the temperature distribution

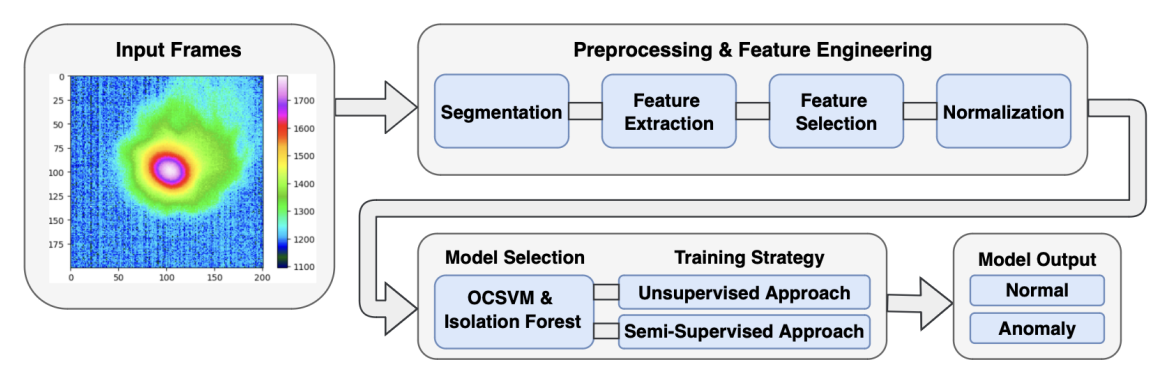


Figure 1: Overview of the proposed methodology.

within each melt pool image, including mean (μ) , median, maximum, minimum, standard deviation (σ) , skewness (1), kurtosis (2), and interquartile range. These measurements quantify the central tendency, dispersion, and shape characteristics of the temperature profile.

Skewness =
$$\frac{1}{nm\sigma^3} \sum_{i=1}^{n} \sum_{j=1}^{m} (T_{ij} - \mu)^3$$
 (1)

Kurtosis =
$$\frac{1}{nm\sigma^4} \sum_{i=1}^{n} \sum_{j=1}^{m} (T_{ij} - \mu)^4$$
 (2)

where T_{ij} represents the temperature value at pixel (i, j) in an $n \times m$ thermal image.

- 2) **Gradient Features:** The spatial gradients of temperature were calculated in both *x* and *y* directions to capture thermal transition rates across the melt pool. From the gradient magnitude distribution, we derived the gradient mean, standard deviation, and maximum values, which characterize thermal stability during deposition.
- 3) **Geometric Features:** From the segmented melt pool region, we extracted morphological features including area, perimeter, circularity, aspect ratio, eccentricity, and axis measurements. These geometric attributes capture the melt pool shape characteristics that have been shown to correlate with porosity formation. Additionally, peak temperature locations were identified to enable spatial analysis of thermal hotspots relative to potential defect formation zones.

2.3 Feature Selection

A total of 26 features were initially extracted across the statistical, gradient-based, and geometric categories. To reduce dimensionality, minimize redundancy, and enhance model interpretability, a reduced feature set was selected. Feature selection is based on the Pearson correlation test where highly correlated features (with correlation coefficients greater

than 0.8 in magnitude) were eliminated to minimize redundancy. This yielded a reduced feature subset of 16 features that preserved diversity in representation while minimizing information overlap.

2.4 Normalization

To mitigate the influence of varying feature magnitudes and ensure numerical stability in model training, feature values were standardized using a statistical transformation based on their mean and standard deviation, as in (3). This transformation was particularly important for stabilizing model training, as differences in feature ranges could have disproportionately impacted distance-based methods such as OCSVM. By normalizing the input data, the models were able to learn more generalizable decision boundaries, improving their robustness against fluctuations in thermal imaging conditions (Schölkopf et al., 2001).

$$x' = \frac{x - \mu}{\sigma} \tag{3}$$

where μ and σ denote the mean and standard deviation of the feature, respectively.

2.5 One-Class Support Vector Machine (OCSVM)

OCSVM operates by learning a decision boundary that encapsulates the normal data points, treating observations outside this boundary as anomalies. The algorithm maps input data into a high-dimensional feature space through a kernel function and constructs a hyperplane that maximizes the distance between the origin and the data points.

The OCSVM implementation utilized the Radial Basis Function (RBF) kernel due to its capability to model nonlinear thermal distributions, allowing for accurate detection of porosity-related deviations and defined as in (4).

$$K(x_i, x_j) = \exp(-\gamma ||x_i - x_j||^2)$$
 (4)

where $K(x_i, x_j)$ represents the kernel function applied to the data instances x_i and x_j while γ denotes the kernel coefficient.

In this work, the critical hyperparameters were optimized through grid search with 5-fold cross-validation, focusing primarily on:

- **Kernel Coefficient** *γ***:** It controls the influence radius of support vectors.
- Outlier Fraction v: It establishes an upper bound on the training error rate and a lower bound on the fraction of support vectors.

The decision function for classifying a new observation x is formulated as in (5).

$$f(x) = \operatorname{sign}(\sum_{i=1}^{n} \alpha_i K(x_i, x) - \rho)$$
 (5)

where α_i represents the Lagrange multipliers, x_i denotes the support vectors, and ρ is the bias term. The sign function serves as a thresholding mechanism that maps the continuous output of the decision function into a binary classification. Observations with f(x) = 1 are considered to conform to the distribution of normal (non-defective) melt pool images, whereas those with f(x) = -1 are classified as anomalies—indicating thermal patterns suggestive of potential porosity. This function thus constitutes the final layer of the OCSVM architecture, enabling interpretable defect classification critical to real-time quality assurance in DED processes.

2.6 Isolation Forest (iForest)

iForest is an ensemble-based anomaly detection algorithm that leverages decision trees to identify anomalies. In contrast to traditional approaches—such as one-class classification—that aim to model normal behavior, iForest adopts a different strategy by directly targeting the isolation of anomalous instances. This method is built on the premise that anomalies are infrequent with distinct characteristics, making them easier to separate from the rest of the data.

iForest offers several notable advantages. It is computationally efficient and scales effectively to large and high-dimensional datasets. Additionally, it requires only minimal and straightforward hyperparameter tuning. Combined with its fully unsupervised nature—which removes the need for labeled data—these characteristics make iForest a highly practical and versatile choice for anomaly detection tasks.

The iForest algorithm involves repeatedly dividing the data space through random selections of features and respective split values. It builds an ensemble of binary trees, referred to as isolation trees (iTrees), where each tree is constructed by choosing a feature at random and then selecting a split value uniformly between its observed minimum and maximum. This recursive partitioning proceeds until either each data point is isolated in its own leaf node or a prespecified maximum tree depth is attained.

For any data instance, its path length refers to the number of splits—or edges—encountered as it travels from the root of an isolation tree to the leaf node where it is ultimately isolated. Because anomalies are typically rare and possess feature values that set them apart from the majority of the data, they are more likely to be separated early in the tree-building process. As a result, anomalous instances tend to exhibit shorter average path lengths across the ensemble of isolation trees. This average path length serves as the basis for computing an anomaly score for each instance, with shorter paths corresponding to higher anomaly scores and indicating a higher likelihood of being anomalous.

As with OCSVM, the critical hyperparameters were optimized via grid search with 5-fold cross-validation, and they include:

- Number of Estimators (Trees): It controls the ensemble size and stability of anomaly score estimates.
- Contamination Parameter: It estimates the proportion of anomalies expected in the data, influencing the decision threshold.

The decision function for classifying a new observation x is as in (6).

$$f(x) = \begin{cases} \text{anomaly,} & \text{if } s(x) \ge \text{threshold} \\ \text{normal,} & \text{otherwise} \end{cases}$$
 (6)

where s(x) represents the average anomaly score across all isolation trees. Higher scores indicate greater deviation from normal melt pool patterns.

3 RESULTS AND DISCUSSION

3.1 Dataset Description

The dataset used in this study is sourced from Zamiela et al. (Zamiela et al., 2023a). The dataset comprises in-process thermal melt pool images and postfabrication porosity labels for Ti-6Al-4V thin-walled structures, fabricated using the OPTOMEC Laser Engineered Net Shaping (LENSTM) 750 system. The

data was collected for nondestructive thermal characterization of laser DED, enabling the development of predictive models for quality control.

Thermal imaging was captured using a Stratonics dual-wavelength pyrometer, which records a top-down view of the melt pool and heat-affected zone, measuring temperatures above 1660 °C. Internal porosity defects were labeled using Nikon X-Ray Computed Tomography (XCT) XT H225, providing reference measurements for lack of fusion defects occurring within the fabricated structure.

The dataset consists of 1,564 cropped pyrometer melt pool images in CSV format, each with a resolution of 200 × 200 pixels. The dataset includes binary porosity labels (0 = No Porosity, 1 = Porosity) with 1,493 non-defective samples and 71 defective samples, creating a highly imbalanced dataset with approximately 4.5% defect occurrence rate. Representative normal and anomalous thermal images are shown in Figure 2. Each thermal image in the dataset is accompanied by metadata including frame number, timestamp, spatial coordinates, melt pool characteristics, and when applicable, porosity size ranging from 0.05 mm to 0.98 mm. The dataset was split into 80% training and 20% testing. Additionally, the models were trained using two different settings:

- 1. **Semi-Supervised Setting:** The training set contains only normal (i.e., non-anomalous) samples, consisting of 1,194 normal images, which account for approximately 80% of the total available normal data. In this one-class training paradigm, both models are trained to learn the underlying distribution and characteristic patterns of normal behavior. During inference, any test sample that exhibits a substantial deviation from the learned normal distribution is flagged as anomalous by the models.
- 2. **Unsupervised Setting:** The training set comprises both normal and anomalous samples, accounting for approximately 80% of the entire dataset. Specifically, it includes 1,194 normal images and 57 anomalous images.

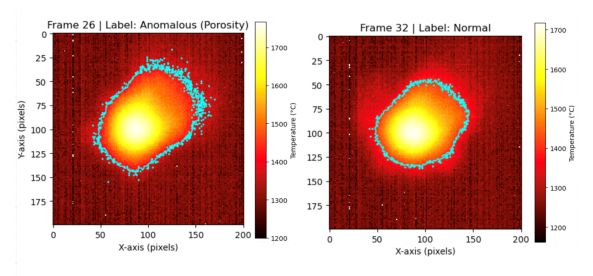


Figure 2: Comparison of the thermal images of the melt pool images in a normal frame and an anomalous (porosity) frame.

This dual training strategy allowed us to evaluate the effect of training data composition on model performance. The impact of these training strategies on model performance is analyzed in the following section, considering their effects on classification metrics, false positive rates, and overall anomaly detection accuracy.

3.2 Findings

3.2.1 Correlation Matrix Analysis

The correlation matrix in Figure 3 helps us understand relationships between different features and provides insights about the dataset, making it easier to choose the most useful ones for anomaly detection in DED. A few key takeaways are as follows:

- Feature Redundancy: Some features, like *mean*, *median*, and *Q1*, are almost identical (correlation coefficients ≥ 0.98). Keeping just one of them simplifies the model without losing information. The same applies to features like *variance* and *standard deviation*.
- Effect on Model Performance: Filtering out redundant features improves model accuracy. Models trained on the selected features outperformed those using all features (see Tables 1 and 2), with iForest handling variability better than OCSVM, which was more sensitive to training data changes.

3.2.2 Classification Metrics

Table 1 and Table 2 summarize the performance metrics for the OCSVM and iForest models, respectively. The evaluation was conducted using different feature sets and training settings.

For OCSVM, the selected feature set yielded the best results under the semi-supervised scheme, achieving a precision of 0.76, a recall of 0.97, and an F1-score of 0.85. However, performance dropped significantly in the unsupervised scheme, where precision and F1-score fell to 0.44, and 0.56, respectively. This suggests that OCSVM is highly sensitive to training data consistency and may not generalize well under unsupervised settings.

Similarly, iForest performed best with the selected features under the semi-supervised scheme, proving that the semi-supervised approach works better at capturing anomalies for these models. With a precision of 0.82, a recall of 0.96, and an F1-score of 0.88. Unlike OCSVM, iForest maintained relatively better performance under the unsupervised scenario, with an

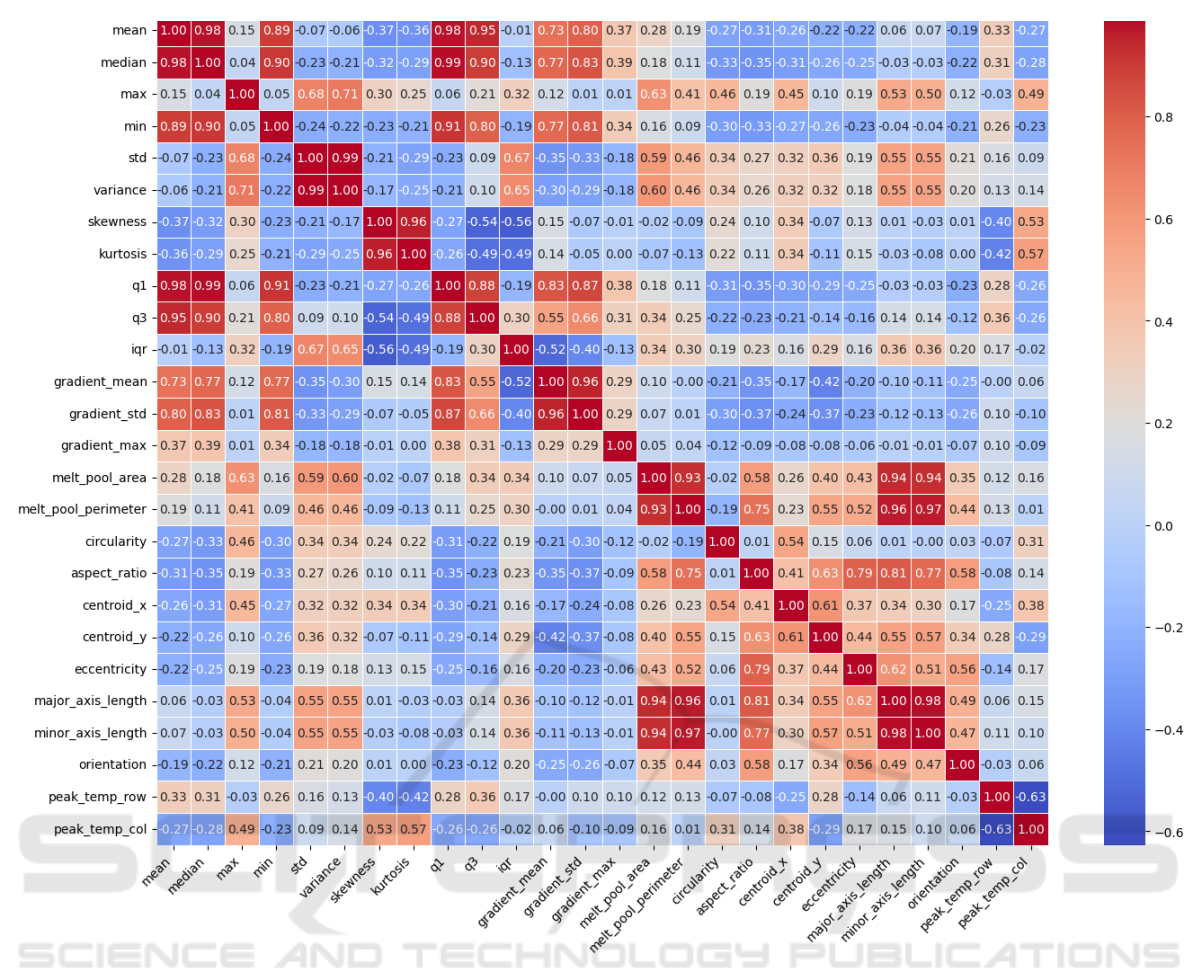


Figure 3: Feature correlation matrix.

Table 1: Results of One-Class SVM (OCSVM).

Feature Set	Training	Precision	Recall	F1	Accuracy
All Features	Semi-Supervised	0.75	0.96	0.84	0.93
	Unsupervised	0.39	0.67	0.49	0.93
Selected Features	Semi-Supervised	0.76	0.97	0.85	0.93
	Unsupervised	0.44	0.77	0.56	0.94

Table 2: Results of Isolation Forest.

Feature Set	Training	Precision	Recall	F1	Accuracy
All Features	Semi-Supervised	0.81	0.91	0.86	0.94
	Unsupervised	0.62	0.68	0.64	0.96
Selected Features	Semi-Supervised	0.82	0.96	0.88	0.95
	Unsupervised	0.74	0.84	0.78	0.98

F1-score of 0.78, indicating its robustness to varying data distributions.

Overall, using the selected features proved superior for both models, highlighting their effectiveness in capturing relevant information. Additionally, iForest demonstrated greater resilience to the unsuper-

vised scheme compared to OCSVM, making it a more reliable choice in scenarios with data variability.

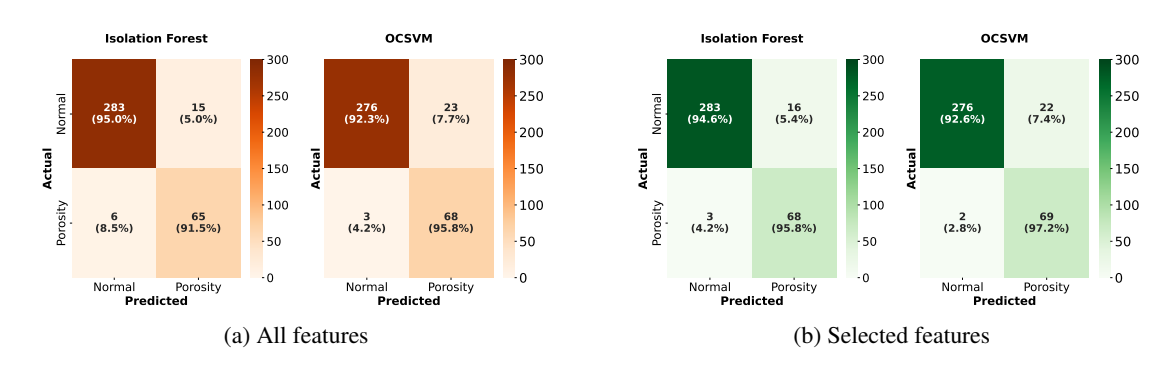


Figure 4: Confusion matrices for the ML models (semi-supervised setting).

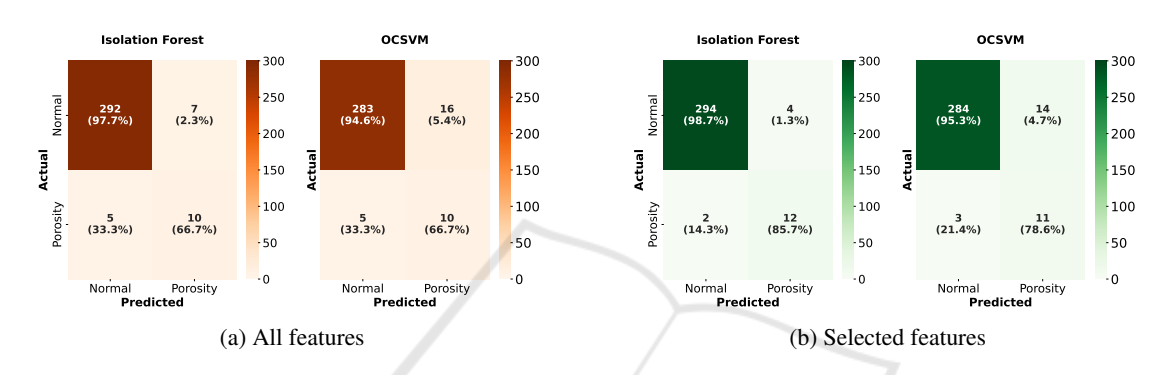


Figure 5: Confusion matrices for the ML models (unsupervised setting).

3.2.3 Confusion Matrix Analysis

The confusion matrices (see Figures 4 and 5) illustrate the classification performance of iForest and OCSVM under different feature sets and training paradigms. Each confusion matrix represents the average results obtained over 5-fold cross-validation, ensuring robustness and mitigating performance fluctuations due to dataset variability. These matrices allow for a direct comparison of the models in terms of their ability to correctly identify normal and anomalous samples. The following key observations are drawn from the confusion matrices:

Comparison of the Best Results for iForest and OCSVM: iForest demonstrated a high recall of 95.8%, successfully identifying 68 out of 71 porosity cases (refer to Figure 4b), emphasizing its strong sensitivity to defects. Additionally, it achieved a precision of 82%, with 16 normal samples misclassified as defective. These results lead to an F1-score of 0.88, which reflects a strong balance between detecting defects and limiting false positives. In contrast, OCSVM exhibited a slightly higher recall of 97.2%, detecting 69 out of 71 porosity cases, but with a lower precision of 75.82%, as it misclassified 22 normal samples as porosity. These results indicate that iForest prioritizes capturing more true defect cases while

maintaining a better balance between false positives and false negatives, making it more reliable in scenarios where reducing unnecessary false alarms is critical. On the other hand, OCSVM slightly increases recall at the expense of more false positives, which may introduce additional costs in practical DED applications.

Effect of Feature Selection: Feature selection played a crucial role in the trade-off between precision and recall. For iForest, using the selected features resulted in a recall of 95.8%. This indicates that the model correctly detected 68 out of 71 porosity cases, with a false positive rate of approximately 5.4% (refer to Figure 4b). On the other hand, when all features were used, recall significantly decreased to 91.5%, with a false positive rate of roughly 5%, yielding a lower detection rate for defective instances (refer to Figure 4a). This performance improvement indicates that reducing feature redundancy allowed the model to better distinguish between normal and defective cases.

Effect of Training Settings: The training scheme significantly influenced the overall model performance, affecting both recall and precision. For OCSVM, the semi-supervised approach achieved a precision of 75.8% and a recall of 97.2%, leading to an F1-score of 85.1%, demonstrating its strong abil-

ity to identify defective cases while maintaining a relatively low false positive rate (see Table 1 and Figure 4b). However, under the unsupervised setting, performance deteriorated significantly, with precision dropping to 44% and recall decreasing to 78.6%, resulting in an F1-score of 56.4% (see Table 1 and Figure 5b). This decline indicates that exposure to mixed data introduced classification uncertainty, causing the model to struggle with distinguishing between normal and defective instances. Similarly, for iForest (see Table 2 and Figure 4b), training on normal data (semi-supervised) resulted in a precision of 82%, a recall of 95.8%, and an F1-score of 87.7%, highlighting a strong balance between false positive reduction and defect detection sensitivity. In contrast, when trained under the unsupervised setting, precision declined to 74%, recall dropped to 85.7%, and the F1-score decreased to 78% (see Table 2 and Figure 5b). While iForest demonstrated more robustness than OCSVM, it still exhibited reduced classification confidence under the unsupervised scheme, leading to increased false positives. These findings indicate that semi-supervised training with exclusively normal data enhances both recall and precision, ensuring more reliable defect detection in DED processes. In contrast, the unsupervised setting, while more flexible, introduces noise and weakens model performance, particularly in recall and precision trade-offs.

4 CONCLUSION

This work adopted a semi-supervised anomaly detection approach for defect detection in DED processes. It is based on two effective semi-supervised algorithms: iForest and OCSVM. The results for both algorithms were compared with an unsupervised setting to highlight the effectiveness of the adopted semisupervised approach. The results demonstrate that the semi-supervised setting, where the training data exclusively includes normal data, significantly enhances detection performance, as evidenced by higher precision, recall, and an associated F1-score compared to the unsupervised setting. Comparing the individual algorithms, iForest consistently outperforms OCSVM in this defect detection task for both settings. In the semi-supervised setting, iForest achieved an F1-score of 0.88 and a respective accuracy of 95%. Notably, correlation-based feature selection improved the models' effectiveness by removing redundancy and noise. Specifically, it provided the most robust and stable performance across both normal-only and mixed-data training conditions. These findings underscore the robustness of the semi-supervised approach for anomaly detection with the notorious data imbalance issue. It also emphasizes the critical importance of feature selection strategies, training data quality, and algorithm choice in achieving optimal anomaly detection outcomes. The proposed approach is highly adaptable and can be seamlessly extended to defect detection in other additive manufacturing processes, such as powder bed fusion.

REFERENCES

- Alexopoulou, V. E. (2021). Study and modeling of the transition from conduction to keyhole mode during SLM process. Master's thesis, School of Mechanical Engineering, National Technical University of Athens.
- Dass, A. and Moridi, A. (2019). State of the art in directed energy deposition: From additive manufacturing to materials design. *Coatings*, 9(7).
- Era, I. Z., Zhou, F., Raihan, A. S., Ahmed, I., Abul-Haj, A., Craig, J., Das, S., and Liu, Z. (2024). In-situ melt pool characterization via thermal imaging for defect detection in directed energy deposition using vision transformers. arXiv preprint arXiv:2411.12028.
- Farea, S. M., Unel, M., and Koc, B. (2024). Defect prediction in directed energy deposition using an ensemble of clustering models. In *Proceedings of the 2024 IEEE 22nd International Conference on Industrial Informatics (INDIN)*, pages 1–6.
- Gaja, H. and Liou, F. (2018). Defect classification of laser metal deposition using logistic regression and artificial neural networks for pattern recognition. *Interna*tional Journal of Advanced Manufacturing Technology, 94(1-4):315–326.
- García-Moreno, A.-I. (2019). Automatic quantification of porosity using an intelligent classifier. *International Journal of Advanced Manufacturing Technology*, 105(5):1883–1899.
- Herzog, T., Brandt, M., Trinchi, A., et al. (2024). Defect detection by multi-axis infrared process monitoring of laser beam directed energy deposition. *Scientific Re*ports, 14:3861.
- Hespeler, S., Dehghan-Niri, E., Juhasz, M., and Luo, K. (2022). Deep learning for in-situ layer quality monitoring during laser-based directed energy deposition (LB-DED) additive manufacturing process. *Applied Sciences*, 12(18):8974.
- Khanzadeh, M., Chowdhury, S., Marufuzzaman, M., Tschopp, M. A., and Bian, L. (2018). Porosity prediction: Supervised-learning of thermal history for direct laser deposition. *Journal of Manufacturing Systems*, 47:69–82.
- Li, S. H., Kumar, P., and Chandra, S. (2023). Directed energy deposition of metals: Processing, microstructures, and mechanical properties. *International Materials Reviews*, 2023.
- Qin, J., Hu, F., Liu, Y., Witherell, P., and Wang, C. C. L. (2022). Research and application of machine learning

- for additive manufacturing. *Additive Manufacturing*, 52:102014.
- Schölkopf, B., Platt, J. C., Shawe-Taylor, J., Smola, A. J., and Williamson, R. C. (2001). Estimating the support of a high-dimensional distribution. *Neural Computation*, 13(7):1443–1471.
- Taheri, H., Koester, L. W., Bigelow, T. A., Faierson, E. J., and Bond, L. J. (2019). In situ additive manufacturing process monitoring with an acoustic technique: clustering performance evaluation using k-means algorithm. *Journal of Manufacturing Science and Engi*neering, 141(4).
- Tang, D., He, X., Wu, B., Wang, X., Wang, T., and Li, Y. (2022). The effect of porosity defects on the midcycle fatigue behavior of directed energy deposited Ti-6Al-4V. Theoretical and Applied Fracture Mechanics, 2022.
- Zamiela, C., Tian, W., Guo, S., and Bian, L. (2023a). Thermal-porosity characterization data of additively manufactured ti–6al–4v thin-walled structure via laser engineered net shaping. Harvard Dataverse. Available at: https://doi.org/10.7910/DVN/BWHYEH.
- Zamiela, C., Tian, W., Guo, S., and Bian, L. (2023b). Thermal-porosity characterization data of additively manufactured Ti–6Al–4V thin-walled structure via laser engineered net shaping. *Data in Brief*, 51:109722.
- Zhao, X., Imandoust, A., Khanzadeh, M., Imani, F., and Bian, L. (2021). Automated anomaly detection of laser-based additive manufacturing using melt pool sparse representation and unsupervised learning. In *Solid Freeform Fabrication Symposium*.